Δ133p53 and Δ160p53 isoforms of the tumor suppressor protein p53 exert dominant-negative effect primarily by co-aggregation

Liuqun Zhao[1], Tanel Punga[2], Suparna Sanyal[1*]

[1]Department of Cell and Molecular Biology, Uppsala University, Biomedical Center, SE-75124, Uppsala, Sweden

[2]Department of Medical Biochemistry and Microbiology, Uppsala University, Biomedical Center, SE-75123, Uppsala, Sweden

[*]Corresponding author e-mail: suparna.sanyal@icm.uu.se

Abstract

p53 is a tumor suppressor protein with multiple isoforms that have shared or specific functions. However, two of its isoforms, Δ133p53 and Δ160p53, with large N-terminal deletions, can aggressively cause cancer. These isoforms exert a dominant negative effect on full-length p53 (FLp53), although the precise molecular mechanisms are unknown. Here, we investigated the mechanisms of action of Δ133p53 and Δ160p53 isoforms using chromatin immunoprecipitation, luciferase expression, subcellular fractionation, and immunofluorescence assays. Our study elucidates that these DNA-binding deficient p53 isoforms form hetero-tetrameric complexes with FLp53 and disrupt FLp53's DNA binding and transcriptional activities when present in a higher proportion than FLp53 in the tetramer. However, these structurally unstable isoforms promote vigorous protein aggregation involving FLp53, disrupting its structure and sequestering it in the cytoplasmic and nuclear aggregates, thereby limiting its availability to function as a transcription activator protein. Thus, co-aggregation of Δ133p53 and Δ160p53 with FLp53, rather than hetero-tetramerization, is the primary factor contributing to their dominant-negative effect. Modulating the stability and aggregation of p53 isoforms could be a novel strategy for cancer therapy.

Keywords: p53, Δ133p53, Δ160p53, dominant-negative effect, protein aggregation

Introduction

The tumor suppressor protein p53 is an essential transcription activator protein modulating the expression of multiple target genes. By regulating various cellular processes such as cell cycle arrest, apoptosis, senescence, DNA repair, and angiogenesis, p53 prevents cancer development[1, 2]. The intricate p53 pathway is stimulated by various stress stimuli, including DNA damage and oncogene activation, which lead to the stabilization and activation of the p53 protein[3]. Stabilized p53 acts as a transcription activator protein as it can directly bind to its response elements (REs) and recruit different transcription co-activator proteins at various gene promoters[4]. One of the best-known p53 targets is the p21 (also known as CIP1, WAF1) gene promoter, which contains two p53REs and is efficiently activated by the p53 protein[5, 6]. The encoded p21 protein blocks cell cycle progression and thereby executes tumor suppressor activity of the p53 protein[7, 8].

The TP53 gene produces at least twelve distinct p53 isoforms: p53 (α, β, γ), Δ40p53 (α, β, γ), Δ133p53 (α, β, γ), and Δ160p53 (α, β, γ). It has been shown that the p53 isoforms contribute to the regulation of the p53 pathway by regulating the expression of p53 target genes[9, 10, 11]. Notably, p53 isoforms exhibit both overlapping and distinct functions compared to the canonical p53[11, 12, 13] and have been reported to promote tumor progression in various cancers[11, 14]. The p53 isoforms are generated through alternative promoter usage, alternative splicing, and alternative transcription starting site usage[9, 15]. Notably, these isoforms differ from the full-length (FL) p53 (canonical p53, p53α) by lacking variable segments of the N-terminus (N-terminal isoforms: Δ40, Δ133, and Δ160) and possessing alternative C-terminus (C-terminal isoforms - α, β, and γ). The FLp53 protein consists of four primary functional domains: transactivation domains (TAD-1 and TAD-2), DNA-binding core domain (DBD), nuclear localization sequence (NLS), and the oligomerization domain (OD)[16]. Native FLp53 typically functions as a tetrameric protein, where the individual monomers bind cooperatively to DNA[17, 18]. The C-terminal truncated isoforms (β/γ-isoforms) lacking the OD have lower transactivation activity because of reduced tetramerization efficiency[19, 20, 21, 22]. In contrast, the N-terminal truncated isoforms (α-isoforms), which retain the entire C-terminal OD, can form a complex with FLp53 and exert dominant-negative effects on p53's transcriptional activity[23, 24, 25]. Important for the present study are two p53 isoforms: Δ133p53 and Δ160p53. The Δ133p53 protein lacks both TADs and a part of the first conserved cysteine box of the DBD, whereas the Δ160p53 protein lacks both TADs and the entire

first conserved cysteine box of the DBD[9, 26]. The relatively well-characterized Δ133p53 isoform can inhibit p53-dependent apoptosis by directly interacting with the FLp53[23, 27, 28]. The Δ133p53 protein can also modulate the expression of p53 target genes, such as p21 and miR-34a, thereby controlling cellular senescence[24]. Therefore, Δ133p53 plays a vital role in antagonizing p53-mediated tumor suppression. The oncogenic function of the newly identified Δ160p53 isoform is less known, although it is associated with p53 mutation-driven tumorigenesis[29] and in melanoma cells' aggressiveness[30]. Whether or not the Δ160p53 isoform also impedes FLp53 function in a similar way as Δ133p53 is an open question.

The precise molecular mechanisms involved in the biological function of the Δ133p53 and the Δ160p53 proteins, especially how they exert dominant-negative effects on FLp53, remain poorly understood. In this study, we have analyzed the DNA-binding, transcriptional activity, and oligomerization capacity of the human FLp53, Δ133p53, and Δ160p53 proteins. Our data show that the Δ133p53 and Δ160p53 proteins are deficient in binding to p53-regulated promoters and inducing expression of the p53 target genes. Moreover, the Δ133p53 and Δ160p53 isoforms can form hetero-oligomers with FLp53 and inhibit FLp53 function in a concentration-dependent manner. Two potential mechanisms for their pro-oncogenic activity are suggested: (i) the formation of hetero-tetramers with FLp53, inhibiting its DNA-binding and transcriptional activity, and (ii) the aggregation property of the isoforms leading to co-aggregation of the FLp53 protein. Interestingly, while hetero-tetramerization partially attenuates p53 activity, the co-aggregation of FLp53 with Δ133p53 and Δ160p53 emerges as the predominant factor contributing to the dominant-negative effect.

Results

Δ133p53 and Δ160p53 proteins exhibit structural destabilization, exposure of hydrophobic surface and high propensity to aggregation.

The DBD, also known as the core domain of the FLp53 protein (human p53, residues 94-292) has a structure with an aggregation-prone sequence (residues 251–257)[31] (Figure 1A). The core domain contains a hydrophobic core of β-sandwich, which consists of two antiparallel β-sheets with four strands (S1, S3, S8, and S5) and five strands (S6, S7, S4, S9, and S10) respectively[32] (Supplementary Figure 1A). The DNA-binding surface is constituted by two large loops (L2 and L3) and a loop–sheet–helix (LSH) motif, which comprises loop L1, a β-sheet formed by the β-hairpin S2–

S2′, the C-terminal residues of strand S10, and the α-helix H2[33] (Supplementary Figure 1A). Compared to FLp53, the N-terminal deletion isoforms Δ133p53 and Δ160p53 lack the entire TADs (Figure 1A), which are crucial for recruiting transcription co-activator proteins[34]. In addition, the Δ133p53 protein is missing the β-strand S1 in the β-sandwich and a part of the LSH motif (L1, S2, and the N-terminal residue 132 of the strand S2′) in the DBD (Supplementary Figure 1A). The Δ160p53 protein, on the other hand, lacks a part of the β-sandwich (β-strands S1, S3, and N-terminal residues 156-159 of S4) and a part of the LSH motif (L1 and β-hairpin S2–S2′) (Supplementary Figure 1A). Therefore, the N-terminal deletion affects the structural integrity of both the β-sandwich and the LSH motif in the core domain.

To assess the structural impact of the N-terminal deletions in FLp53, we analyzed the contact information derived from the core domain of FLp53 (PDB ID: 3KMD) structure[35]. We observed that both Δ133p53 and Δ160p53 lack several crucial contacts between the N- and C-terminal regions in FLp53 (Figure 1B). For Δ133p53, the contact between the L1 and S2 segments in the N-terminal region and the α-helix H2 in the C-terminal region within the LSH motif is disrupted (Figure 1B, insert 1), suggesting a potential impairment of the stabilizing of DNA-binding interface. For Δ160p53, in addition to the missing contact between L1, S2 and H2, there are also no contacts between the S2′ segment in the N-terminal region and the S10 and H2 segments in the C-terminal region within the LSH motif (Figure 1B, insert 2), as well as between S4 and S7 or S9 in the β-sandwich core domain (Figure 1B, inserts 3 and 4). These contacts are crucial for maintaining the structural integrity and folding of the core domain. Therefore, both Δ133p53 and Δ160p53 will likely have a partially or fully destabilized core domain that may impair their DNA-binding ability.

We predicted the monomer structure of Δ133p53 and Δ160p53 by Alphafold2[36] (Supplementary Figure 1B). Hydrophobic surface analysis revealed that Δ133p53 and Δ160p53 exposed four highly hydrophobic residues (L252, I254, I255, and L257) within the aggregation-prone sequence, while FLp53 exposes only one residue (L252) (Figure 1C). This increased hydrophobicity may induce the aggregation of Δ133p53 and Δ160p53. Moreover, Δ133p53 and Δ160p53 have a partial or complete structural loss of the β-hairpin S2–S2′ (Supplementary Figure 1A), which restricts access to the hydrophobic core[37]. This structural alteration results in an enhanced exposure of the hydrophobic core of the β-sandwich domain compared to FLp53 (Figure 1C). This exposure potentially facilitates the

propensity for protein aggregation, as suggested by previous studies[37, 38] as well as our *in vitro* aggregation assay with purified FLp53, Δ133p53 and Δ160p53 proteins (Supplementary Figure 2). In summary, these findings suggest that the large N-terminal deletion in Δ133p53 and Δ160p53 would compromise the structural stability of FLp53 and induce aggregation, with Δ160p53 being more severely affected among the two.

Δ133p53 and Δ160p53 form complexes with FLp53 and display aggregation propensity.

To investigate the oligomerization properties of Δ133p53 and Δ160p53, which retain the OD known to facilitate p53 tetramerization[39], we performed immunoprecipitation assays with the FLAG epitope-tagged p53 proteins. For that purpose, the C-terminal FLAG-tagged FLp53, Δ133p53, and Δ160p53 proteins were overexpressed in p53-deficient H1299 cells and purified with an anti-FLAG antibody. All FLAG-tagged proteins were efficiently immunoprecipitated and showed the expected migration pattern on the SDS-PAGE (Supplementary Figure 3A). Notably, higher molecular weight forms of Δ133p53 and Δ160p53 were observed in SDS-PAGE (Supplementary Figure 3A). As aggregates are resistant to SDS and heat treatment, this suggests that, unlike FLp53, these isoforms have a higher propensity to form aggregates. To rule out the possibility that the FLAG epitope might contribute to this aggregation, similar experiments were performed with the V5-tagged p53 proteins. Notably, similar aggregates were detected under identical experimental conditions (Supplementary Figure 3B), confirming that the observed aggregation behavior of Δ133p53 and Δ160p53 was not an artifact introduced by the antibody epitope tags.

To further examine the impact of N-terminal truncations on oligomer formation, we co-expressed the aforementioned FLAG-tagged p53 proteins as the baits along with the V5-tagged FLp53, Δ133p53, and Δ160p53 proteins as preys. The V5-tagged FLp53, Δ133p53, and Δ160p53 proteins specifically interacted with their corresponding FLAG-tagged proteins (Figure 2A, lanes 1–6), demonstrating their capacity to form homo-oligomers (Figure 2B). In addition, interactions between FLp53-FLAG/Δ133p53-V5, FLp53-FLAG/Δ160p53-V5, Δ133p53-FLAG/Δ160p53-V5, and Δ160p53-FLAG/Δ133p53-V5 were found (Figure 2A, lanes 7–10), suggesting that they can also form hetero-oligomers (Figure 2B). These findings are consistent with previous studies indicating that Δ40p53 can hetero-oligomerize with FLp53[40, 41]. Notably, the FLAG- and V5-tagged Δ133p53 or Δ160p53 proteins formed aggregates on reducing SDS-PAGE (Figure 2A, lanes 5–10), confirming our initial

observations (Supplementary Figure 3). Taken together, these data show that Δ133p53 and Δ160p53 can oligomerize with FLp53 and each other, and they exhibit a marked tendency to form insoluble aggregates.

Δ133p53 and Δ160p53 negatively influence FLp53's DNA-binding activity.

Previous studies have shown that the p53 lacking the TADs and the PRD (ΔNp53DBD, residues 94-393) retain full DNA-binding capacity as the FLp53[42, 43]. In contrast, the Δ133p53 (residues 133-393) and Δ160p53 (residues 160-393) isoforms additionally lack part of the DBD (residues 94-292). This deficiency raises questions about the impact of partial DBD deletion on the DNA-binding activity of p53. To address this question, we performed a chromatin immunoprecipitation (ChIP) assay to measure the DNA-binding activity of FLp53 and its isoforms Δ133p53 and Δ160p53 to several known p53 targeted promoters controlling proteins regulating cycle arrest (p21), protein stability (MDM2), and apoptosis induction (BAX and PUMA) (Figure 3A). Previous studies have classified p53 DNA-binding affinities. Accordingly, the p21 promoter has the highest affinity, the MDM2 promoter has moderate affinity, whereas the BAX and PUMA promoters show relatively low p53-binding affinity[44, 45, 46]. Consistent with these findings, our results revealed distinct binding affinities of the FLp53 protein to these target gene promoters (Figure 3B). Notably, the Δ133p53 and Δ160p53 isoforms demonstrated a significant loss of DNA-binding activity at these promoters (Figure 3B).

We subsequently hypothesized that Δ133p53 and Δ160p53 might compromise the DNA-binding ability of FLp53 through hetero-oligomer formation (Figure 2). To study this, we co-transfected FLp53 along with either Δ133p53 or Δ160p53 expressing plasmid and measured FLp53's binding to the aforementioned promoters. The presence of Δ133p53 or Δ160p53 significantly reduced the binding of FLp53 to the p21 promoter, which has the highest affinity for FLp53, while having minimal impact on its interaction with the other promoters (Figure 3C). These findings suggest that Δ133p53 and Δ160p53 isoforms may selectively impair the ability of FLp53 to bind to high-affinity target promoters.

Δ133p53 and Δ160p53 impede FLp53-mediated transcription activation.

The p53-mediated transcription activation depends on its binding ability to specific p53REs at the target gene promoters[47, 48]. To evaluate the influence of the FLp53 protein interaction with its isoforms, Δ133p53 and Δ160p53, on transcription, we employed a luciferase reporter assay with the p21,

MDM2, BAX, and PUMA promoters fused to a firefly luciferase reporter gene. As expected, all four promoters were responsive to FLp53-mediated transcriptional activation (Figure 4A-D). Notably, FLp53 activation of the PUMA promoter was relatively low, possibly due to the lower binding affinity of FLp53 to the PUMA promoter (Figure 3B). In contrast, neither Δ133p53 nor Δ160p53 activated any tested promoters (Figure 4A-D), indicating a lack of functional capability to stimulate transcription from these promoters.

In order to assess how Δ133p53 and Δ160p53 influence FLp53-mediated transcription on different p53-responsive promoters, we co-expressed FLp53 along with increasing amounts of Δ133p53 or Δ160p53 in H1299 cells. We found that co-expression of FLp53 with Δ133p53 or Δ160p53 at a 1:1 ratio did not significantly alter the activation of the p21 and MDM2 promoters compared to FLp53 alone (Figure 4A and B). This result suggests that at an equal protein expression ratio (Figure 2A), these isoforms did not exert a dominant-negative effect on the FLp53 at these promoters. However, a strong reduction in BAX promoter activation was evident under the same experimental condition (Figure 4C), suggesting that the isoforms can disrupt FLp53 function on the BAX promoter. Interestingly, both isoforms enhanced the activation of the PUMA promoter when added with FLp53 in a 1:1 ratio (Figure 4D).

Adjusting the ratio of FLp53 to isoforms to 1:5 revealed that higher isoform expression levels significantly impaired FLp53-mediated activation of the p21, MDM2, and BAX promoters (Figure 4A-C). Interestingly, Δ133p53 at a 1:5 ratio had almost no impact on PUMA promoter activity, whereas Δ160p53 reduced it compared to FLp53 alone (Figure 4D). These results indicate that higher expression ratios of Δ133p53 and Δ160p53 relative to FLp53 might be required to exert dominant-negative effects. To test this hypothesis, we escalated the ratio of FLp53 to isoforms to 1:10. As expected, the activity of all four promoters decreased significantly at this ratio (Figure 4A-D). Notably, Δ160p53 showed a more potent inhibitory effect than Δ133p53 at the 1:5 ratio on all promoters except for the p21 promoter, where their impacts were similar (Figure 4E-H). However, at the 1:10 ratio, Δ133p53 and Δ160p53 had similar effects on all transactivation except for the MDM2 promoter (Figure 4E-H). This differential impact underscores the variability in how p53 isoforms influence FLp53 function across different promoters and expression ratios. Collectively, these findings demonstrate that isoforms with impaired DNA-binding capability can indeed exert dominant-negative effects on the

function of FLp53, with the magnitude of this impact being promoter-specific and dependent on the relative expression levels of the proteins.

The Δ133p53 and Δ160p53 proteins affect the subcellular localization and aggregation of FLp53.

p53 exerts its transcriptional activity in the nucleus, and its appropriate subcellular localization is crucial for regulating p53 functions[49]. Immunoblotting analysis with isolated nuclear and cytoplasmic fractions revealed distinct subcellular localization patterns for the FLp53 and its isoforms Δ133p53 and Δ160p53 (Figure 5A and B). The nuclear levels of Δ133p53 and Δ160p53 were similar to those of FLp53; however, the cytoplasmic levels of Δ133p53 and Δ160p53 were approximately 1.8-fold higher than those of FLp53 (Figure 5B). These results suggest that Δ133p53 and Δ160p53 exhibit a greater tendency for cytoplasmic localization.

Immunofluorescence analysis of the cells expressing FLp53 and the two isoforms confirmed the above-observed protein localization pattern (Figure 5C). The FLp53 protein was predominantly localized in the nucleus, with minimal to no fluorescence signal detected in the cytoplasm (Figure 5C, panel 1 and Supplementary Figure 4, panels 1 and 2). In contrast, the Δ133p53 and Δ160p53 proteins exhibited reduced nuclear staining and enhanced cytoplasmic staining relative to FLp53, with Δ160p53 showing more pronounced cytoplasmic staining (Figure 5C). Notably, Δ133p53 and Δ160p53 demonstrated a heterogeneous distribution in the nucleus and cytoplasm (Figure 5C, panels 2 and 3). Furthermore, both Δ133p53 and Δ160p53 exhibited predominantly cytoplasmic punctate staining, particularly Δ160p53, suggesting the formation of protein aggregates (Figure 5C, panels 2 and 3).

Given that p53 aggregation has been found in numerous tumor cells[50, 51, 52, 53], it is important to explore the effects of Δ133p53 or Δ160p53 isoforms on the aggregation of FLp53. To investigate the aggregation property of the p53 isoforms, we performed a biochemical fractionation of the H1299 cells expressing FLp53 along with Δ133p53 or Δ160p53 at 1:5 ratio. Notably, our fractionation approach allows us to analyze soluble cytoplasmic and nuclear fractions as well as insoluble nuclear fraction. Immunoblotting of the soluble fraction showed that an excess of Δ133p53 and Δ160p53 isoforms reduced the levels of FLp53 in both the cytoplasm and nucleus, with a notable reduction in the nucleus (Figure 6A and C). Conversely, insoluble nuclear FLp53 increased significantly upon co-

expression with the p53 isoforms, with Δ160p53 showing a more prominent effect (Figure 6B and D, Supplementary Figure 5). These results collectively demonstrate that Δ133p53 and Δ160p53 isoforms strongly induce FLp53 aggregation, and the decrease in soluble FLp53 levels could be attributed to its aggregation when co-expressed with isoforms Δ133p53 and Δ160p53. We complemented the immunoblotting assays with immunofluorescence assays. Our results clearly show the co-localization of FLp53 with the isoforms Δ133p53 and Δ160p53. More importantly, we find co-aggregation of FLp53 with the two isoforms forming punctate spots in the cytoplasm and nucleus (Figure 6E, panels 2 and 3 and Supplementary Figure 4, panels 3 and 4). Furthermore, more prominent subnuclear foci of FLp53 formed in the cells co-expressing the Δ160p53 protein (Figure 6E, panel 3 and Supplementary Figure 4, panel 4), which were detected in the Δ133p53 protein expressing H1299 cells. Thus, these results imply that Δ133p53 and Δ160p53 isoforms efficiently induce co-aggregation of FLp53, potentially influencing its function in cancer cells.

Discussion

The inactivation of p53 is one of the most common events in cancer cells[54]. Functionally compromised p53 mutations are prevalent in more than half of human cancers[55, 56]. Specific p53 isoforms have recently been associated with tumorigenesis in various cancer types[11, 14]. The aberrant expression of Δ133p53 has been found in colorectal cancer[24, 57] and lung cancer[58]. In comparison, the oncogenic role of the Δ160p53 isoform in human cancers is less explored[11], although links have been established between the expression of Δ160p53 isoform and melanoma cells[30]. The mechanisms of the oncogenic potential of p53 isoforms have attracted increasing attention from researchers[14, 59, 60, 61, 62, 63]. A theory of the dominant-negative effect has been introduced, but its exact details have remained unknown.

The ChIP and luciferase activity assays show that the isoforms Δ133p53 and Δ160p53 are defective in their ability to bind DNA and activate transcription (Figure 3B and Figure 4A-D). A possible reason for the diminished DNA-binding function of these isoforms is that their core domains are defective (Figure 1B). The Δ133p53 and Δ160p53 isoforms lack approximately 20% and 33% of the DBD, which hinders their ability to bind to p53REs. We find that co-expression of Δ133p53 and Δ160p53 with FLp53 exerts an inhibitory effect on FLp53's DNA-binding ability (Figure 3C). However, the degree to which Δ133p53 and Δ160p53 impair FLp53 function is influenced by both the

expression levels of these isoforms and the specific promoters of the target genes (Figure 4). For the p21 and MDM2 promoters, equal expression of FLp53 and the two isoforms didn't show much effect. However, higher expression levels of the isoforms gradually inhibited FLp53's activity to induce transcription from those promoters (Figure 4A and B). Notably, the PUMA promoter behaved differently, whereby 1:1 co-expression of FLp53 with Δ133p53 or Δ160p53 significantly increased its activity (Figure 4D). We speculate that this isoform expression level may activate p21 induction pathways independent of FLp53[64], potentially facilitating the interaction between FLp53 and p21, which is required for optimal activation of PUMA promoter activity[65]. These results underscore a complex regulatory network where FLp53 and the isoform expression levels, target gene specificity, and transcriptional activities modulate p53-mediated cellular responses.

Our co-expression data clearly indicate that the isoforms Δ133p53 and Δ160p53 exert a dominant-negative effect on FLp53 function (Figures 3 and 4). Since both of these p53 isoforms are defective in DNA binding and they possess an intact C-terminal OD, it is not unexpected that they form different species of homo- and hetero-tetramers with FLp53. In accordance with that, the immunoprecipitation assays using FLAG-tagged FLp53 and V5-tagged Δ133p53 or Δ160p53 demonstrate a potential direct interaction between these isoforms and FLp53 (Figure 2A, lanes 7 and 8). However, in what ratio the p53 isoforms impose inhibition to FLp53 function is worth investigating. We employed a theoretical model of p53 (hetero)-tetramer activity in transcriptional activation from p21, MDM2, BAX, and PUMA promoters by varying relative expression levels of the isoforms[66] (Supplementary Figure 6). We assumed that the transfection level was a good proxy for the expression level. Interestingly, the experimental inhibition curves with Δ133p53 or Δ160p53 derived from the luciferase reporter assay were all above the theoretical inhibition curves for two isoform molecules per tetramer (Supplementary Figures 6B-E), suggesting that at least three isoform molecules per tetramer are required to abolish the transcriptional activity of FLp53. This is similar to an earlier report with Δ40p53 isoform, which was shown to exert a dominant-negative effect at a 3:1 ratio with FLp53[41].

Interestingly, similar to Δ40p53[60], the Δ133p53, and Δ160p53 proteins can aggregate in the cytoplasm (Figures 5C and 6E). Due to cytoplasmic aggregation, only a limited amount of these isoforms can successfully be imported into the nucleus successfully. Additionally, the isoforms tend to aggregate within the nucleus (Figures 6B and E). Consequently, the ratio of these isoforms to FLp53

diminishes in the nucleus in contrast to their expression levels. This decrease reduces the likelihood of forming hetero-tetramers, in which the isoforms will be in higher proportion than FLp53. Thus, it seems unlikely that hetero-tetramerization of Δ133p53 and Δ160p53 isoforms with FLp53 would be the main reason for their dominant-negative effect.

Next we investigated whether aggregation of the Δ133p53 and Δ160p53 isoforms contributes to their functional loss and dominant-negative effect on FLp53. Our immunofluorescence and immunoprecipitation analyses of H1299 cells expressing these isoforms show a higher aggregation propensity of the two isoforms than FLp53 (Figure 5C and Supplementary Figures 2 and 3A). The aggregation likely results from the exposure of hydrophobic sequences in the isoforms (Figure 1C). In addition, the absence of N-terminal TADs in Δ133p53 and Δ160p53 isoforms may prevent their MDM2-mediated ubiquitin-proteasome degradation[54, 67]. This may, in turn, lead to higher accumulation of Δ133p53 and Δ160p53 isoforms in the cell, which, combined with an unstable core domain, promotes their aggregation.

More interestingly, our immunofluorescence and immunoprecipitation assays demonstrate large co-aggregation of FLp53 with Δ133p53 and Δ160p53 isoforms in the cytoplasm as well as in the nucleus when expressed together (Figure 6B and E and Supplementary Figure 4, panels 3 and 4). The predominant cytoplasmic aggregation would sequester FLp53 in the cytoplasm. Moreover, it may destabilize FLp53's conformation, potentially masking the nuclear localization sequence (NLS) and preventing its nuclear import[68]. Additionally, it may disrupt the interaction of FLp53 with MDM2, thereby inhibiting its MDM2-induced degradation and enhancing its accumulation[69], which would drive it more to the aggregation pathway. All these processes involving FLp53 aggregation would result in reduction of the functional FLp53 in the cell and more importantly, in the nucleus. Cytoplasmic aggregation would also limit the isoforms from nuclear import, reducing the possibility of heteroterramerization. Therefore, we propose that the co-aggregation of Δ133p53 and Δ160p53 with FLp53 is the primary factor for their dominant-negative effect. This mechanism is consistent with the model where structural mutations, such as R175H and R282W in FLp53, induce co-aggregation and exert a dominant-negative effect[31].

We propose a model to explain how the p53 isoforms Δ133p53 and Δ160p53 inhibit FLp53 activity and exert dominant-negative effect on it (Figure 7A). Two mechanisms are involved: a subsidiary

mechanism in which Δ133p53 and Δ160p53 isoforms form hetero-tetramers with FLp53 impairing its DNA-binding and transcriptional activities, and a predominant mechanism in which these isoforms promote co-aggregation with FLp53 and abolish its transcriptional activities by disrupting its structure, regulation and degradation pathways. Since elevated levels of Δ133p53 and Δ160p53 relative to FLp53 attenuate its transcriptional activity (Figure 7B, left) and overexpression of FLp53 relative to the isoforms allows to regain it (Figure 7B, right), the tumor-suppressive efficacy of p53 must depend on the balanced expression of FLp53 and its isoforms, highlighting the importance of their relative abundance in cancer cells. Based on our results and recent related publications[60, 63] we propose that co-aggregation, rather than hetero-tetramerization, is the primary mechanism for the dominant-negative effect exerted by the p53 isoforms with large N-terminal truncations.

Methods

Cell culture, plasmids, and plasmid transfections. Human non-small cell lung carcinoma cells H1299 (p53-null) were obtained from ATCC and cultured in Dulbecco's modified Eagle's medium (DMEM) supplemented with 10% fetal bovine serum (FBS, Thermo Fisher Scientific) and penicillin-streptomycin solution (PEST; Thermo Fisher Scientific) at 37 °C in a 5% CO_2 incubator. The plasmid pcDNA3.1-FLp53-FLAG, encoding human full-length p53 (amino acids 1-393), was synthesized by GenScript (Rijswijk, Netherlands). A flexible linker $(GGGGG)_1$ was introduced between the FLp53 coding sequence and the C-terminal FLAG epitope tag. Subsequently, this fusion construct was inserted into the pcDNA3.1 vector at the NdeI and EcoRI restriction enzyme sites. The plasmids encoding N-terminally truncated p53 proteins (Δ133p53 and Δ160p53) were created by deleting the N-terminal 132 and 159 amino acids from the FLp53 sequence, respectively. To create plasmids expressing C-terminal V5-tagged proteins (FLp53, Δ133p53, and Δ160p53), the respective DNA sequences were amplified by PCR from the pcDNA3.1-FLp53-FLAG template and inserted into the EcoRI and XhoI sites of the pcDNA3.1-V5. Luciferase reporter plasmids, WWP/p21-Luc (Plasmid #16451)[6], pGL3-MDM2-Luc (Plasmid #32365)[70], and PUMA Frag1-Luc (Plasmid #16591)[71] were obtained from Addgene. For the construction of the BAX-Luc reporter plasmid, the p53 binding site in the BAX promoter was PCR amplified from HepG2 genomic DNA kindly provided by Dr. Gang Pan (Uppsala University) and cloned into the pGL3-Basic plasmid (Promega) using XhoI and HindIII sites. The PCR primers used for cloning are listed in Supplementary Table 1. All plasmid transfections were

performed with jetPRIME® (Polyplus) transfection reagent according to the manufacturer's protocol.

Immunoprecipitation and Western blotting. H1299 cells were seeded in a 6-well plate and transfected with 2 µg of various plasmids. The total amount of plasmids (2 µg/well) was kept constant in all samples by adding empty plasmid pcDNA3.1. To investigate p53 oligomerization, cells were co-transfected with equal amounts (1 µg each) of FLAG- and V5-tagged plasmids. After 24 h post-transfection (hpt), cells were harvested and lysed in RIPA buffer (50 mM Tris-HCl pH 7.4, 150 mM NaCl, 1% Triton X-100, 1% sodium deoxycholate, 0.1% SDS, and 1 mM EDTA) supplemented with the Halt Protease Inhibitor Cocktail (Thermo Fischer Scientific) as previously described[72]. The whole cell lysates were incubated for 30 min on ice and centrifuged at 13,000 × g for 15 min at 4°C. A fraction of the cleared cell lysates was reserved as the input sample; the remaining lysates were used for immunoprecipitation with anti-FLAG M2 magnetic beads (Sigma, Cat No. M8823) overnight at 4°C. The beads were washed with 4 ×1 ml of RIPA buffer. Proteins were then eluted from the beads using 2 × Laemmli Sample buffer, separated on a 10% SDS-PAGE, transferred onto nitrocellulose membranes (Bio-Rad), and blocked with 5% nonfat dry milk in TBS containing 0.1% Tween-20 (TBST) for 1 h at room temperature. The blocked membranes were incubated overnight at 4°C with the anti-FLAG (Sigma, Cat No. F2555) and anti-V5 (Sigma, Cat No. V8012) primary antibodies in a blocking buffer overnight at 4°C. Proteins were detected with the IRDye 680RD Goat anti-Rabbit IgG and IRDye 800CW Donkey anti-Mouse IgG secondary antibodies (Li-COR Biosciences). The Western blots were visualized using an Odyssey CLX imaging system (Li-COR Biosciences).

Chromatin immunoprecipitation (ChIP) assays. H1299 cells were seeded in 10 cm cell culture dishes and transfected with 5 µg of either pcDNA3.1-FLp53-FLAG, pcDNA3.1-Δ133p53-FLAG, pcDNA-Δ160p53-FLAG or an empty vector pcDNA3.1 for 24 h. To investigate the impacts of isoforms Δ133p53 and Δ160p53 on the DNA-binding activity of FLp53, H1299 cells were co-transfected with 2.5 µg of pcDNA3.1-FLp53-FLAG along with either 2.5 µg of pcDNA3.1-Δ133p53-V5, pcDNA3.1-Δ160p53-V5 or an equal amount of empty vector pcDNA3.1. The ChIP assays were performed as described previously[73], with minor modification. Briefly, cells were fixed with 1% formaldehyde in PBS for 10 min at room temperature, followed by lysis in 250 µl of lysis buffer (50 mM Tris-HCl pH 8.0, 10 mM EDTA, 1% SDS) supplemented with Halt Protease Inhibitor Cocktail. Lysates were then sonicated for 15 cycles (30 s ON/30 s OFF) using the Bioruptor Pico (Diagenode). The resulting

soluble cell lysates were diluted with dilution buffer (16.7 mM Tris-HCl pH 8.0, 167 mM NaCl, 1.2 mM EDTA, 0.01% SDS, 1.1% Triton X-100) and immunoprecipitated overnight at 4°C with the anti-FLAG M2 magnetic beads. After a series of washes, protein-DNA complexes were eluted, and the crosslinks were reversed through incubation with RNase A (Thermo Fischer Scientific) at 37°C for 30 min, followed by proteinase K (Invitrogen) digestion at 65°C overnight. The enrichment of specific DNA fragments was evaluated with qPCR analysis using HOT FIREPol EvaGreen qPCR Supermix (Solis Biodyne). All qPCR reactions were done in triplicate, employing the QuantStudio™ 6 Flex Real-Time PCR System (Thermo Fisher Scientific). The relative fold enrichments were calculated after normalizing to the input values and considering the pcDNA3.1 transfected samples as 1. Primer sequences used for qPCR analysis are listed in Supplementary Table 1.

Luciferase assay. H1299 cells were seeded in 24-well plates and transfected in triplicate with 25 ng/well of luciferase reporter plasmids and various p53-expressing plasmids. Co-transfection ratios for FLp53 and its isoforms Δ133p53 or Δ160p53, were set at 1:1 (12.5 ng/well of FLp53 to 12.5 ng/well of isoform), 1:5 (12.5 ng/well of FLp53 to 62.5 ng/well of isoform), and 1:10 (12.5 ng/well of FLp53 to125 ng/well of isoform). The total plasmid amount (300 ng/well) was kept consistent across the various groups by supplementing with the empty pcDNA3.1 plasmid. Cells were harvested 24 hpt and lysed in a Passive Lysis Buffer (Promega). The cell lysate was centrifuged at 13,000 × g for 5 min at 4°C, and 20 µl of the lysate was analyzed in triplicates using an Infinite 200 PRO plate reader (TECAN). The luciferase activity of the FLp53 and its isoforms transfected samples was normalized against that of samples transfected with the control vector pcDNA3.1 to obtain relative reporter activity. Results represent the mean values and standard deviations of three independent experimental replicates. The data was analyzed using Origin 2018 software (Origin Lab Corporation, USA).

Subcellular fractionation. The subcellular fractionation assay was carried out using NE-PER Nuclear and Cytoplasmic Extraction Reagents (Thermo Fischer Scientific), with minor modifications. In brief, H1299 cells were seeded in 10 cm cell culture dishes and transfected with 0.8 µg of the following plasmids: pcDNA3.1-FLp53-FLAG, pcDNA3.1-Δ133p53-FLAG, pcDNA-Δ160p53-FLAG, and the control vector pcDNA3.1. To investigate the effects of overexpressing p53 isoforms on the subcellular localization of FLp53, co-transfection was performed using FLAG-tagged FLp53 and V5-tagged Δ133p53 or Δ160p53 at a 1:5 ratio (0.8 µg to 4.2 µg). Cells were transfected with 5 µg of the

empty vector pcDNA3.1 as a control. About 24 hpt, cells were collected by trypsinization, resuspended in ice-cold CER I buffer containing Halt Protease Inhibitor Cocktail and incubated for 10 min on ice. Subsequently, ice-cold CER II buffer was added according to the manufacturer's instructions. The cytoplasmic extracts were isolated by centrifugation at 14,000 × g for 5 min at 4°C. The nuclear pellet was then resolved in ice-cold RIPA buffer supplemented with Halt Protease Inhibitor Cocktail, subjected to vortex for 15 s every 10 min for a total of 40 min, and centrifuged at 14,000 × g for 10 min to obtain the soluble nuclear fraction. The insoluble nuclear pellet (i.e., insoluble nuclear fraction) was resuspended in RIPA buffer, an appropriate volume of 2 × Laemmli Sample buffer was added, and the samples were heated at 95°C until the pellet fully dissolved. For Western blot experiments, equal volumes of each subcellular fraction were separated by SDS-PAGE, and the nitrocellulose membranes were probed with the respective antibodies. Histone H3 (nuclear marker) and α-Tubulin (cytoplasmic marker) antibodies were used to verify the purity of the nuclear and cytoplasmic fractions. All primary antibodies: anti-FLAG (Sigma, Cat No. F2555), anti-V5 (Sigma, Cat No. V8012 and Cat No. AB3792), anti-Histone H3 (Abcam, Cat No. ab1791), and anti-α-Tubulin (Sigma, Cat No. T6199) were incubated on membranes overnight at 4°C. The Western blots were visualized using an Odyssey CLX imaging system, and the proteins were quantified using Image Studio Version 5.5 (Li-COR).

Immunofluorescence analysis. H1299 cells were seeded on glass coverslips in 24-well plates and transfected with 250 ng/well of either pcDNA3.1-FLp53-FLAG, pcDNA3.1-Δ133p53-FLAG, pcDNA-Δ160p53-FLAG or the control vector pcDNA3.1. To investigate whether an excess of p53 isoforms could influence the subcellular localization of FLp53, H1299 cells were co-transfected with 250 ng/well of pcDNA3.1-FLp53-FLAG along with 1000 ng/well of pcDNA3.1-Δ133p53-V5, pcDNA3.1-Δ160p53-V5, or pcDNA3.1. About 24 hpt, cells were fixed with 4% paraformaldehyde in PBS, followed by permeabilization with 0.2% Triton X-100 in PBS for 15 min at room temperature as described previously[74]. Fixed cells on coverslips were incubated overnight at 4°C with primary antibodies anti-FLAG (Sigma, Cat No 1804, 1:1000 dilution), and anti-V5 (Sigma, Cat No AB3792, 1:1000 dilution). Subsequently, coverslips were incubated with the Alexa Fluor 488 goat anti-mouse IgG (Invitrogen, Cat No. A11001, 1:2000 dilution) and/or Alexa Fluor 594 chicken anti-rabbit IgG (H+L) (Invitrogen, Cat No. A21442, 1:2000 dilution) secondary antibodies for 30 min at room temperature. The coverslips

were mounted with ProLong Diamond Antifade Mountant (Invitrogen, Cat No. P36961), and nuclei were counterstained using DAPI. Subcellular localization was visualized using a Nikon Eclipse 90i microscope (Nikon, Japan). Images were processed using ImageJ software[75] and subsequently arranged by Inkscape.

Acknowledgments

We thank Dr. Zamaneh Hajikhezri for her help with the immunofluorescence experiments and Dr. Gang Pan for reagents. This research was funded by grants from the Swedish Research Council (2023-05237, 2018-05946 and 2018-05498), from Wenner-Gren Foundation (UPD2023-0185) and from the Knut and Alice Wallenberg Foundation (KAW 2017.0055) to S.S.

Author contribution

S.S. conceived the idea of the project; L.Z. and T.P. performed experiments; L.Z., T.P., and S.S. analyzed the data; L.Z. wrote the manuscript and prepared Figures. All authors reviewed, edited, and approved the manuscript.

Competing interests

The authors declare no competing interests.

References

1. Levine AJ, Oren M. The first 30 years of p53: growing ever more complex. *Nature reviews Cancer* **9**, 749-758 (2009).
2. Vogelstein B, Lane D, Levine AJ. Surfing the p53 network. *Nature* **408**, 307-310 (2000).
3. Pflaum J, Schlosser S, Müller M. p53 Family and Cellular Stress Responses in Cancer. *Frontiers in oncology* **4**, 285 (2014).
4. Sullivan KD, Galbraith MD, Andrysik Z, Espinosa JM. Mechanisms of transcriptional regulation by p53. *Cell death and differentiation* **25**, 133-143 (2018).
5. Macleod KF*, et al.* p53-dependent and independent expression of p21 during cell growth, differentiation, and DNA damage. *Genes & development* **9**, 935-944 (1995).
6. el-Deiry WS*, et al.* WAF1, a potential mediator of p53 tumor suppression. *Cell* **75**, 817-825 (1993).
7. Shamloo B, Usluer S. p21 in Cancer Research. *Cancers* **11**, (2019).

8. Indeglia A, Murphy ME. Elucidating the chain of command: our current understanding of critical target genes for p53-mediated tumor suppression. *Critical reviews in biochemistry and molecular biology*, 1-11 (2024).

9. Joruiz SM, Bourdon JC. p53 Isoforms: Key Regulators of the Cell Fate Decision. *Cold Spring Harbor perspectives in medicine* **6**, (2016).

10. Khoury MP, Bourdon JC. p53 Isoforms: An Intracellular Microprocessor? *Genes & cancer* **2**, 453-465 (2011).

11. Zhao L, Sanyal S. p53 Isoforms as Cancer Biomarkers and Therapeutic Targets. *Cancers* **14**, 3145 (2022).

12. Mehta S*, et al.* Adaptive homeostasis and the p53 isoform network. *EMBO reports*, e53085 (2021).

13. Pal A, Ghosh PK, Das S. The "LINC" between Δ40p53-miRNA Axis in the Regulation of Cellular Homeostasis. *Molecular and cellular biology* **43**, 335-353 (2023).

14. Vieler M, Sanyal S. p53 Isoforms and Their Implications in Cancer. *Cancers* **10**, 288 (2018).

15. Sharathchandra A, Katoch A, Das S. IRES mediated translational regulation of p53 isoforms. *Wiley interdisciplinary reviews RNA* **5**, 131-139 (2014).

16. Khoury MP, Bourdon JC. The isoforms of the p53 protein. *Cold Spring Harbor perspectives in biology* **2**, a000927 (2010).

17. Jeffrey PD, Gorina S, Pavletich NP. Crystal structure of the tetramerization domain of the p53 tumor suppressor at 1.7 angstroms. *Science (New York, NY)* **267**, 1498-1502 (1995).

18. Weinberg RL, Veprintsev DB, Fersht AR. Cooperative binding of tetrameric p53 to DNA. *Journal of molecular biology* **341**, 1145-1159 (2004).

19. Jänicke RU, Graupner V, Budach W, Essmann F. The do's and don'ts of p53 isoforms. *Biological chemistry* **390**, 951-963 (2009).

20. Wang P*, et al.* p53 domains: structure, oligomerization, and transformation. *Molecular and cellular biology* **14**, 5182-5191 (1994).

21. Wang Y, Schwedes JF, Parks D, Mann K, Tegtmeyer P. Interaction of p53 with its consensus DNA-binding site. *Molecular and cellular biology* **15**, 2157-2165 (1995).

22. Kim H*, et al.* p53 requires an intact C-terminal domain for DNA binding and transactivation. *Journal of molecular biology* **415**, 843-854 (2012).

23. Bourdon JC*, et al.* p53 isoforms can regulate p53 transcriptional activity. *Genes & development* **19**, 2122-2137 (2005).

24. Fujita K*, et al.* p53 isoforms Delta133p53 and p53beta are endogenous regulators of replicative cellular senescence. *Nature cell biology* **11**, 1135-1142 (2009).

25. Horikawa I*, et al.* Δ133p53 represses p53-inducible senescence genes and enhances the generation of human induced pluripotent stem cells. *Cell death and differentiation* **24**, 1017-1028 (2017).

26. Pavletich NP, Chambers KA, Pabo CO. The DNA-binding domain of p53 contains the four conserved regions and the major mutation hot spots. *Genes & development* **7**, 2556-2564 (1993).

27. Aoubala M*, et al.* p53 directly transactivates Δ133p53α, regulating cell fate outcome in response to DNA damage. *Cell death and differentiation* **18**, 248-258 (2011).

28. Gong H*, et al.* p73 coordinates with Δ133p53 to promote DNA double-strand break repair. *Cell death and differentiation* **25**, 1063-1079 (2018).

29. Candeias MM, Hagiwara M, Matsuda M. Cancer-specific mutations in p53 induce the translation of Δ160p53 promoting tumorigenesis. *EMBO reports* **17**, 1542-1551 (2016).

30. Tadijan A*, et al.* Altered Expression of Shorter p53 Family Isoforms Can Impact Melanoma Aggressiveness. *Cancers* **13**, (2021).

31. Xu J*, et al.* Gain of function of mutant p53 by coaggregation with multiple tumor suppressors. *Nature chemical biology* **7**, 285-295 (2011).

32. Cho Y, Gorina S, Jeffrey PD, Pavletich NP. Crystal structure of a p53 tumor suppressor-DNA complex: understanding tumorigenic mutations. *Science (New York, NY)* **265**, 346-355 (1994).

33. Joerger AC, Allen MD, Fersht AR. Crystal structure of a superstable mutant of human p53 core domain. Insights into the mechanism of rescuing oncogenic mutations. *The Journal of biological chemistry* **279**, 1291-1296 (2004).

34. Raj N, Attardi LD. The Transactivation Domains of the p53 Protein. *Cold Spring Harbor perspectives in medicine* **7**, (2017).

35. Chen Y, Dey R, Chen L. Crystal structure of the p53 core domain bound to a full consensus site as a self-assembled tetramer. *Structure (London, England : 1993)* **18**, 246-256 (2010).

36. Mirdita M, Schütze K, Moriwaki Y, Heo L, Ovchinnikov S, Steinegger M. ColabFold: making protein folding accessible to all. *Nature methods* **19**, 679-682 (2022).

37. Cañadillas JM, Tidow H, Freund SM, Rutherford TJ, Ang HC, Fersht AR. Solution structure of p53 core domain: structural basis for its instability. *Proceedings of the National Academy of Sciences of the United States of America* **103**, 2109-2114 (2006).

38. Olotu FA, Soliman MES. From mutational inactivation to aberrant gain-of-function: Unraveling the structural basis of mutant p53 oncogenic transition. *Journal of cellular biochemistry* **119**, 2646-2652 (2018).

39. Clore GM*, et al.* Refined solution structure of the oligomerization domain of the tumour suppressor p53. *Nature structural biology* **2**, 321-333 (1995).

40. Courtois S*, et al.* DeltaN-p53, a natural isoform of p53 lacking the first transactivation domain, counteracts growth suppression by wild-type p53. *Oncogene* **21**, 6722-6728 (2002).

41. Hafsi H, Santos-Silva D, Courtois-Cox S, Hainaut P. Effects of Δ40p53, an isoform of p53 lacking the N-terminus, on transactivation capacity of the tumor suppressor protein p53. *BMC cancer* **13**, 134 (2013).

42. Petty TJ*, et al.* An induced fit mechanism regulates p53 DNA binding kinetics to confer sequence specificity. *The EMBO journal* **30**, 2167-2176 (2011).

43. Emamzadah S, Tropia L, Vincenti I, Falquet B, Halazonetis TD. Reversal of the DNA-binding-induced loop L1 conformational switch in an engineered human p53 protein. *Journal of molecular biology* **426**, 936-944 (2014).

44. Weinberg RL, Veprintsev DB, Bycroft M, Fersht AR. Comparative binding of p53 to its promoter and DNA recognition elements. *Journal of molecular biology* **348**, 589-596 (2005).

45. Purvis JE, Karhohs KW, Mock C, Batchelor E, Loewer A, Lahav G. p53 dynamics control cell fate. *Science (New York, NY)* **336**, 1440-1444 (2012).

46. Park SY, Jeong MS, Jang SB. In vitro binding properties of tumor suppressor p53 with PUMA and NOXA. *Biochemical and biophysical research communications* **420**, 350-356 (2012).

47. Menendez D*, et al.* Diverse stresses dramatically alter genome-wide p53 binding and transactivation landscape in human cancer cells. *Nucleic acids research* **41**, 7286-7301 (2013).

48. Beckerman R, Prives C. Transcriptional regulation by p53. *Cold Spring Harbor perspectives in biology* **2**, a000935 (2010).

49. Stommel JM, Marchenko ND, Jimenez GS, Moll UM, Hope TJ, Wahl GM. A leucine-rich nuclear export

signal in the p53 tetramerization domain: regulation of subcellular localization and p53 activity by NES masking. *The EMBO journal* **18**, 1660-1672 (1999).

50. Costa DC, de Oliveira GA, Cino EA, Soares IN, Rangel LP, Silva JL. Aggregation and Prion-Like Properties of Misfolded Tumor Suppressors: Is Cancer a Prion Disease? *Cold Spring Harbor perspectives in biology* **8**, (2016).

51. de Oliveira GA, Rangel LP, Costa DC, Silva JL. Misfolding, Aggregation, and Disordered Segments in c-Abl and p53 in Human Cancer. *Frontiers in oncology* **5**, 97 (2015).

52. Levy CB*, et al.* Co-localization of mutant p53 and amyloid-like protein aggregates in breast tumors. *The international journal of biochemistry & cell biology* **43**, 60-64 (2011).

53. Li J, Guo M, Chen L, Chen Z, Fu Y, Chen Y. Amyloid aggregates induced by the p53-R280T mutation lead to loss of p53 function in nasopharyngeal carcinoma. *Cell death & disease* **15**, 35 (2024).

54. Kussie PH*, et al.* Structure of the MDM2 oncoprotein bound to the p53 tumor suppressor transactivation domain. *Science (New York, NY)* **274**, 948-953 (1996).

55. Hollstein M, Sidransky D, Vogelstein B, Harris CC. p53 mutations in human cancers. *Science (New York, NY)* **253**, 49-53 (1991).

56. Bykov VJN, Eriksson SE, Bianchi J, Wiman KG. Targeting mutant p53 for efficient cancer therapy. *Nature reviews Cancer* **18**, 89-102 (2018).

57. Campbell H*, et al.* ∆133p53 isoform promotes tumour invasion and metastasis via interleukin-6 activation of JAK-STAT and RhoA-ROCK signalling. *Nature communications* **9**, 254 (2018).

58. Fragou A*, et al.* Increased Δ133p53 mRNA in lung carcinoma corresponds with reduction of p21 expression. *Molecular medicine reports* **15**, 1455-1460 (2017).

59. Gong L, Chen J. Δ113p53/Δ133p53 converts P53 from a repressor to a promoter of DNA double-stand break repair. *Molecular & cellular oncology* **3**, e1033587 (2016).

60. Melo Dos Santos N*, et al.* Loss of the p53 transactivation domain results in high amyloid aggregation of the Δ40p53 isoform in endometrial carcinoma cells. *The Journal of biological chemistry* **294**, 9430-9439 (2019).

61. Mondal AM*, et al.* p53 isoforms regulate aging- and tumor-associated replicative senescence in T lymphocytes. *The Journal of clinical investigation* **123**, 5247-5257 (2013).

62. Lei J*, et al.* Conformational stability and dynamics of the cancer-associated isoform Δ133p53β are

modulated by p53 peptides and p53-specific DNA. *FASEB journal : official publication of the Federation of American Societies for Experimental Biology* **33**, 4225-4235 (2019).

63. Arsic N*, et al.* Δ133p53β isoform pro-invasive activity is regulated through an aggregation-dependent mechanism in cancer cells. *Nature communications* **12**, 5463 (2021).

64. Karimian A, Ahmadi Y, Yousefi B. Multiple functions of p21 in cell cycle, apoptosis and transcriptional regulation after DNA damage. *DNA repair* **42**, 63-71 (2016).

65. Kim U, Kim KS, Park JK, Um HD. Involvement of the p53/p21 complex in p53-dependent gene expression. *Biochemical and biophysical research communications* **621**, 151-156 (2022).

66. Chan WM, Siu WY, Lau A, Poon RY. How many mutant p53 molecules are needed to inactivate a tetramer? *Molecular and cellular biology* **24**, 3536-3551 (2004).

67. Chen J, Marechal V, Levine AJ. Mapping of the p53 and mdm-2 interaction domains. *Molecular and cellular biology* **13**, 4107-4114 (1993).

68. Marine JC. p53 stabilization: the importance of nuclear import. *Cell death and differentiation* **17**, 191-192 (2010).

69. Moll UM, Petrenko O. The MDM2-p53 interaction. *Molecular cancer research : MCR* **1**, 1001-1008 (2003).

70. Chang CJ, Freeman DJ, Wu H. PTEN regulates Mdm2 expression through the P1 promoter. *The Journal of biological chemistry* **279**, 29841-29848 (2004).

71. Yu J, Zhang L, Hwang PM, Kinzler KW, Vogelstein B. PUMA induces the rapid apoptosis of colorectal cancer cells. *Molecular cell* **7**, 673-682 (2001).

72. Inturi R, Thaduri S, Punga T. Adenovirus precursor pVII protein stability is regulated by its propeptide sequence. *PloS one* **8**, e80617 (2013).

73. Punga T, Bühler M. Long intronic GAA repeats causing Friedreich ataxia impede transcription elongation. *EMBO molecular medicine* **2**, 120-129 (2010).

74. Kases K*, et al.* The RNA-binding protein ZC3H11A interacts with the nuclear poly(A)-binding protein PABPN1 and alters polyadenylation of viral transcripts. *The Journal of biological chemistry* **299**, 104959 (2023).

75. Schindelin J*, et al.* Fiji: an open-source platform for biological-image analysis. *Nature methods* **9**, 676-682 (2012).

76. Vehlow C*, et al.* CMView: interactive contact map visualization and analysis. *Bioinformatics (Oxford, England)* **27**, 1573-1574 (2011).

77. Meng EC*, et al.* UCSF ChimeraX: Tools for Structure Building and Analysis. *Protein science : a publication of the Protein Society*, e4792 (2023).

78. Goddard TD*, et al.* UCSF ChimeraX: Meeting modern challenges in visualization and analysis. *Protein science : a publication of the Protein Society* **27**, 14-25 (2018).

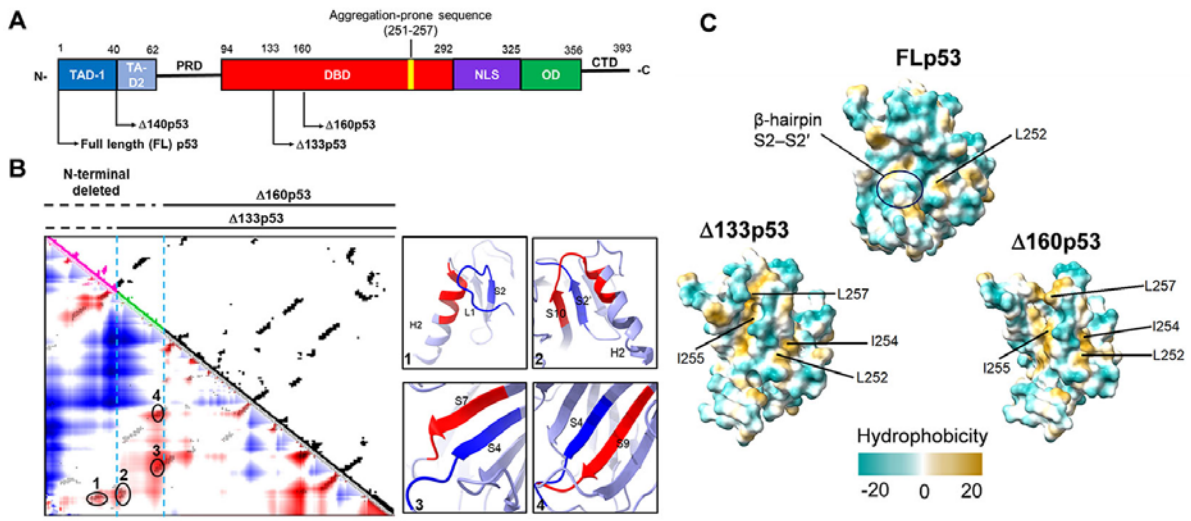

Figure 1. The Δ133p53 and Δ160p53 proteins exhibit structural destabilization.

(A) Schematic domain structures of full-length (FL)p53 and its isoforms. TAD, transactivation domain; PRD, proline-rich domain; DBD, DNA-binding domain; NLS, nuclear localization signal; OD, oligomerization domain; CTD, C-terminal domain. Δ133p53 lacks the entire TAD and approximately 20% of the DBD. Δ160p53 lacks the entire TAD and approximately 33% of the DBD. An aggregation region ILTIITL (residues 251-257) is indicated in the DBD domain. **(B)** Contact density map (C-α 8Å) of the core domain of FLp53 (PDB ID: 3KMD) using CWView[76]. The residues 94-132 and 133-159 were colored magenta and green, respectively. Higher densities are shown in red, and low densities are shown in blue. Among these contacts, four higher-density contacts were selected and shown in oval circles on the map. The corresponding secondary structures of the contacts between the deleted region (blue) and the region (red) in the loop-sheet-helix (LSH) motif or the β-sandwich are shown on the right. **(C)** Comparison analysis of surface hydrophobicity of the core domain in FLp53 (PDB ID: 3KMD) and its isoforms Δ133p53 and Δ160p53 by Chimera X[77, 78]. The exposed hydrophobic residues in the aggregation region ILTIITL (residues 251-257) are labeled. The color scale of hydrophobicity is indicated with the maximum and minimum values in dark cyan and dark goldenrod, respectively. The β-hairpin S2–S2′ was shown in an oval circle.

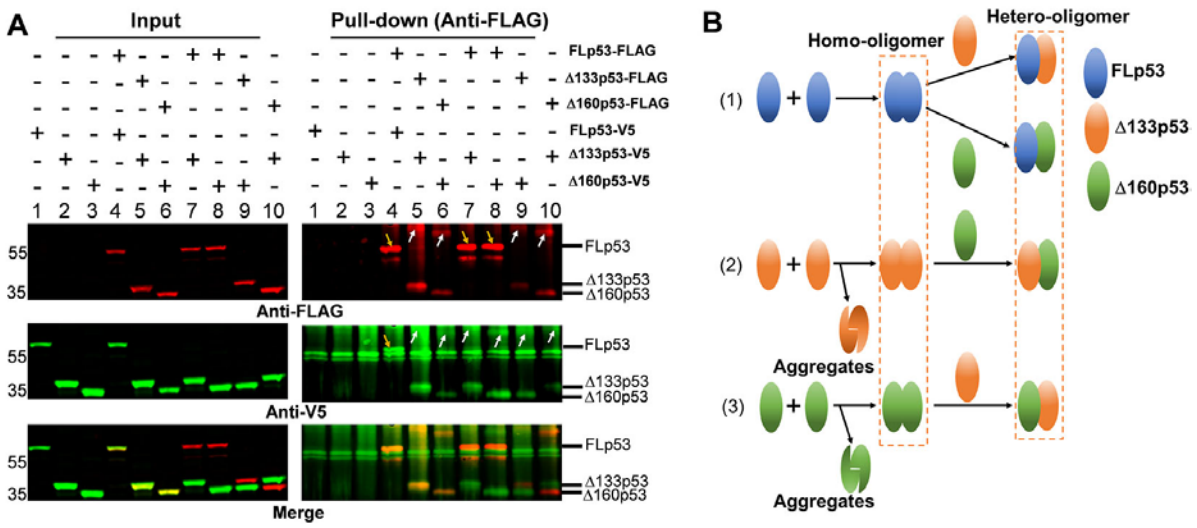

Figure 2. Complex formation among isoforms Δ133p53, Δ160p53, and FLp5 and detection of higher molecular aggregates.

(A) Co-immunoprecipitation of FLp53-FLAG, Δ133p53-FLAG, and Δ160p53-FLAG along with the FLp53-V5, Δ133p53-V5, and Δ160p53-V5 proteins in H1299 cells. The complexes were isolated with anti-FLAG antibody-coupled magnetic beads. Western blot analysis was done with the anti-FLAG (green signal) and anti-V5 (red signal) antibodies. The merged image corresponds to the overlay between the FLAG and V5 antibody signals. Input corresponds to 5% of the whole cell lysate. The higher molecular weight aggregates are marked with white arrows, and the FLp53 protein in lanes 4, 7 and 8 is indicated by yellow arrows. **(B)** A summary of FLp53, Δ133p53, and Δ160p53 oligomerization and aggregation based on data shown in panel A.

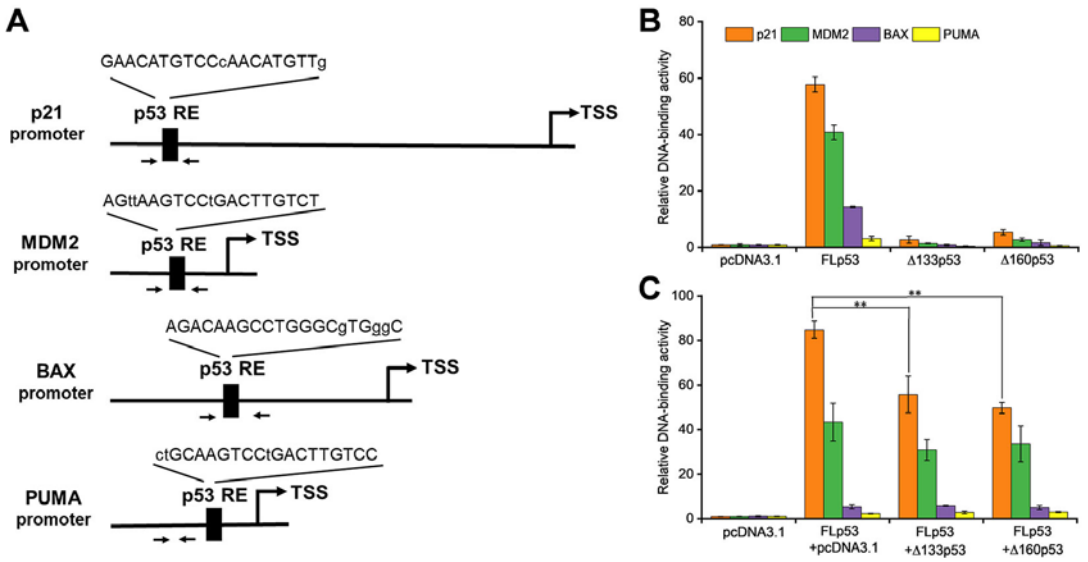

Figure 3. Δ133p53 and Δ160p53 negatively influence FLp53's DNA-binding activity.

(A) Schematic representation of the promoters of p53 target genes (p21, MDM2, BAX, and PUMA). An arrow denotes the transcription start site (TSS). The DNA sequences of p53 response elements (REs) are shown, with uppercase and lowercase letters indicating matched and mismatched bases, respectively, in relation to the canonical p53 RE sequence (RRRCWWGYYY). Paired arrows highlight the regions subjected to quantitative PCR (qPCR) amplification. Specifically, the distal (5') p53 RE within the p21 gene promoter was analyzed. **(B)** Relative DNA-binding of the FLp53-FLAG, Δ133p53-FLAG, and Δ160p53-FLAG proteins to p53 target genes (p21, MDM2, BAX, and PUMA) in H1299 cells. **(C)** Relative DNA-binding of the FLp53-FLAG protein to the p53-target gene promoters in the presence of the V5-tagged protein Δ133p53 or Δ160p53. ChIP-qPCR assay data are shown as relative enrichment of promoter sequences of the target genes after normalization to the control, pcDNA3.1 plasmid transfected cells. Data are represented as the mean of technical triplicates ± standard deviation (SD), $^{**}P < 0.01$ (Student's t-test).

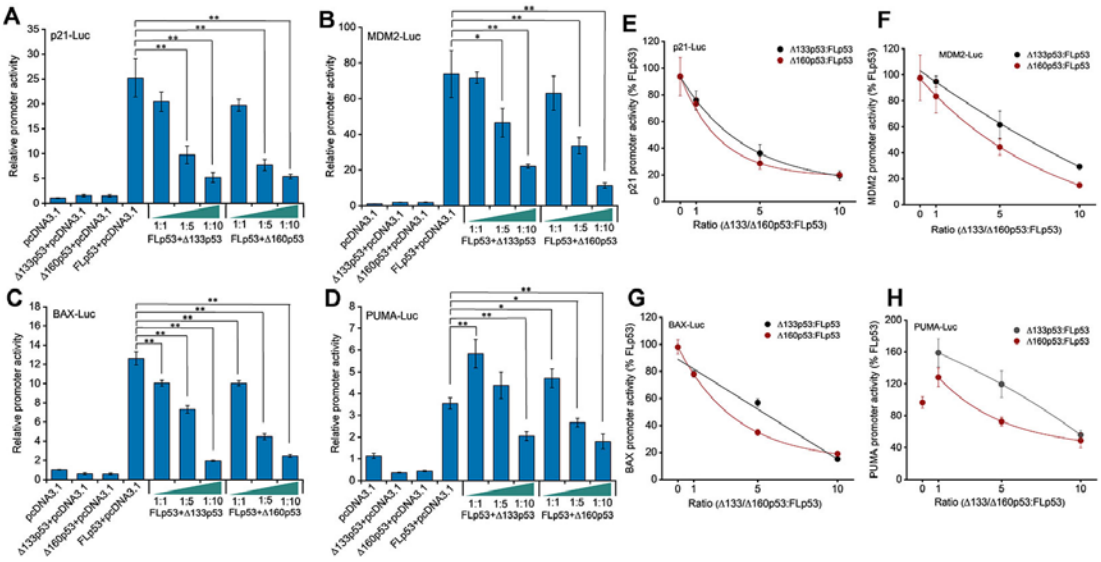

Figure 4. Impact of Δ133p53 and Δ160p53 on FLp53-activated transactivation.

(A-D) H1299 cells were transfected with luciferase reporter plasmids driven by p21 (A), MDM2 (B), BAX (C), and PUMA (D) promoters, along with vectors expressing FLp53, Δ133p53, or Δ160p53. To evaluate the influence of the isoforms on FLp53's transactivation capability, co-expression was performed at ratios of 1:1, 1:5, and 1:10 relative to FLp53. Basal promoter activity was determined by transfecting cells with the empty vector, pcDNA3.1. Relative promoter activity is shown after normalization to the pcDNA3.1-treated sample activity. Data represent mean values ± standard deviation (SD) (n=3). *$P < 0.05$; **$P < 0.01$ (Student's t-test). **(E-H)** The transcriptional activity of FLp53 on the p21 (E), MDM2 (F), BAX (G), and PUMA (H) promoters was inhibited by Δ133p53 and Δ160p53. Inhibition curve fitting was performed using the exponential function ExpDec1 in Origin 2018 software.

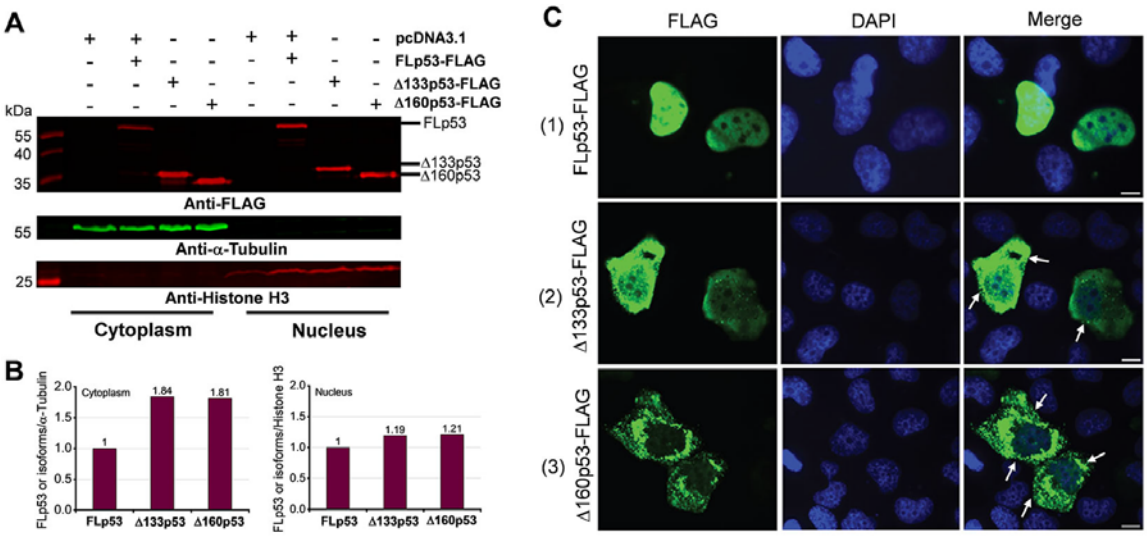

Figure 5. Subcellular distribution of the FLp53, Δ133p53 and Δ160p53 proteins.

(A) Western blot analysis of subcellular fractionation of H1299 cells transfected with the FLAG-tagged FLp53, Δ133p53, or Δ160p53 proteins. Representative immunoblots indicate the presence of these proteins in different cellular fractions. α-Tubulin (cytoplasmic marker) and Histone H3 (nuclear marker) were used to ensure fraction integrity. **(B)** Quantitative bar graph summarizing the protein levels in each fraction. The FLAG-tagged protein levels were normalized to the corresponding fractionation marker (α-Tubulin (cytoplasm) or histone H3 (nucleus)), the relative accumulation of the Δ133p53, or Δ160p53 proteins is shown after considering FLp53 expressing sample as 1. **(C)** Immunofluorescence analysis of H1299 cells expressing FLAG-tagged FLp53, Δ133p53 and Δ160p53. Cell nuclei are visualized with DAPI (blue). The punctate spots (white arrows) indicating protein aggregates are marked. Scale bar, 50 μm.

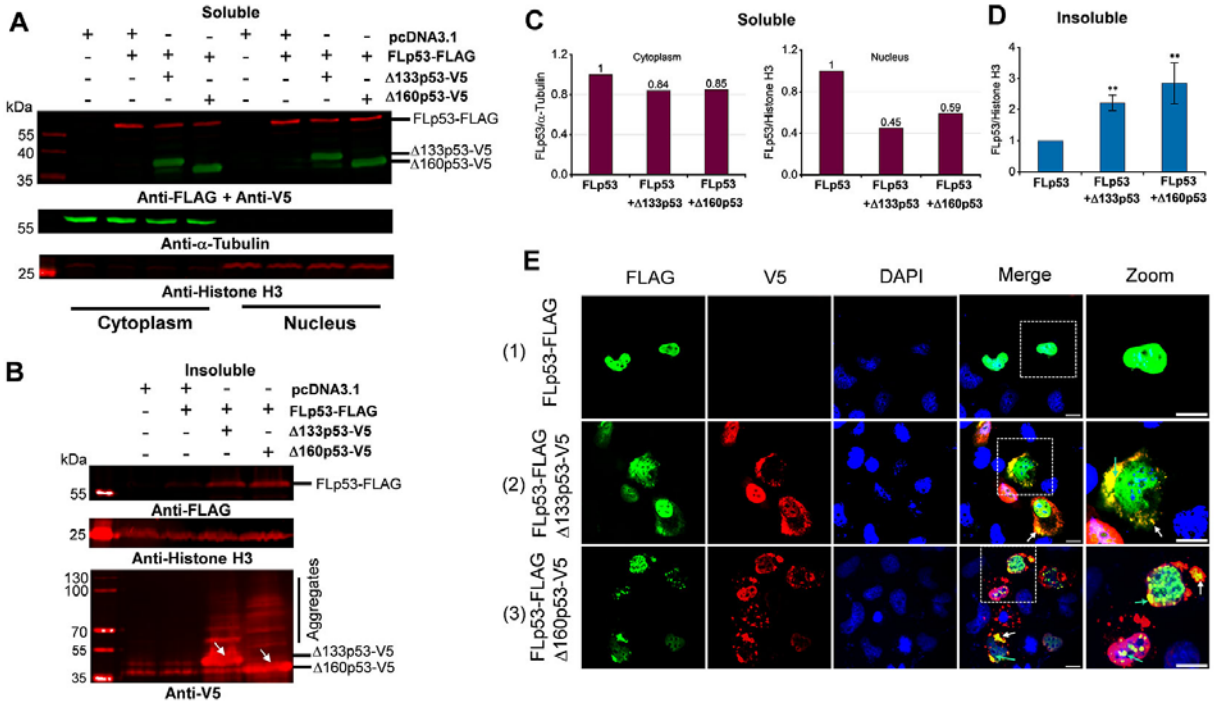

Figure 6. Induction of FLp53 aggregation by Δ133p53 and Δ160p53 isoforms.

(A-B) Western blot analysis of soluble cytoplasmic and nuclear subcellular fractions **(A)** and insoluble nuclear fraction **(B)**. Biochemical fractionation of H1299 cells transfected with the FLAG-tagged FLp53 and V5-tagged Δ133p53 or Δ160p53 at a 1:5 ratio. The aggregated monomers of V5-tagged Δ133p53 and Δ160p53 (indicated by white arrows), as well as the higher molecular weight aggregates, are shown. This figure shows one representative experiment; n=3. **(C)** Quantitative bar graph summarizing the levels of the soluble FLp53-FLAG protein in the cytoplasmic and nuclear fractions. The FLp53-FLAG protein levels were normalized to the corresponding fractionation marker (α-Tubulin or histone H3). Relative accumulation of the FLp53-FLAG in Δ133p53-V5 or Δ160p53-V5 expressing cells is shown after considering the FLp53-FLAG protein expressing sample as 1. **(D)** Quantitative bar graph summarizing the levels of the FLp53-FLAG protein in the insoluble nuclear fraction relative to the histone H3. Data normalization as in panel C, data represent mean values ± standard deviation (SD). $^{**}P < 0.01$ (Student's t-test). **(E)** Immunofluorescence analysis of H1299 cells transfected with FLp53-FLAG alone or in combination with V5-tagged isoforms Δ133p53 and Δ160p53 expressing plasmids at a concentration ratio of 1:5. Cell nuclei were visualized with DAPI (blue). The co-aggregation of isoforms with FLp53 in the cytoplasm (white arrows) and nucleus (bright green arrows) are indicated. Scale bar, 50 μm.

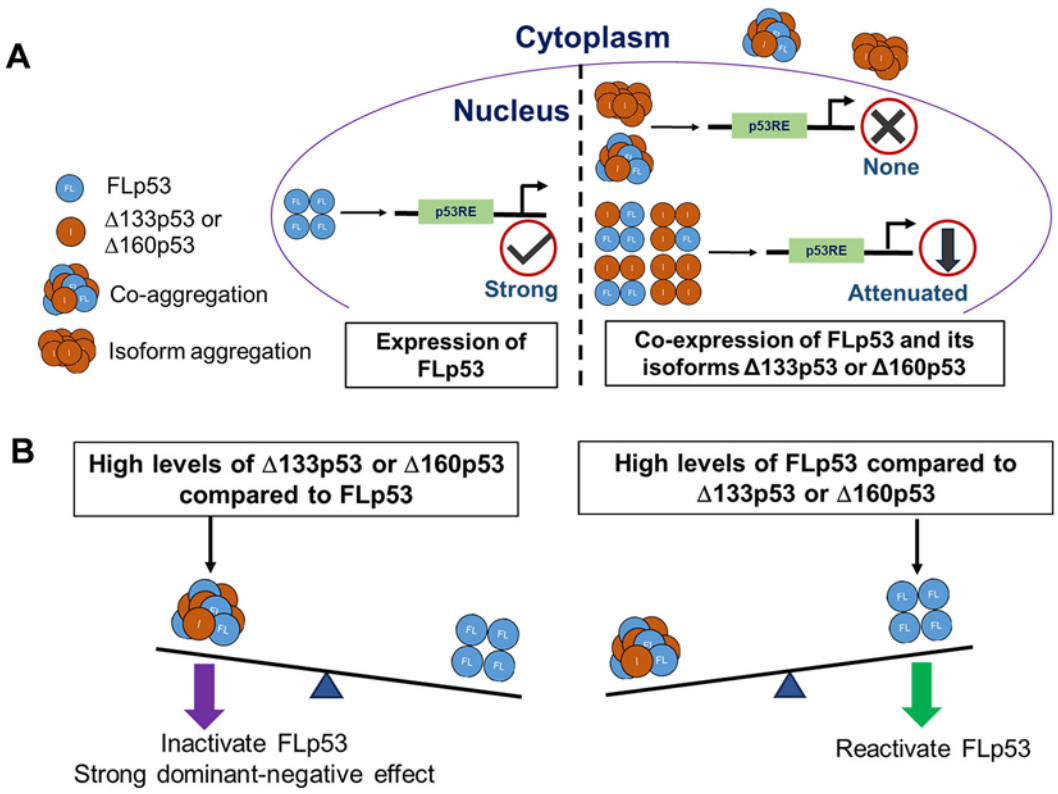

Figure 7. (A) Schematic representation of the underlying mechanisms by which Δ133p53 and Δ160p53 exert dominant-negative effect on FLp53.

(A) When expressed alone, FLp53 demonstrates strong transcriptional activity, but when expressed together with the Δ133p53 or Δ160p53 isoforms, FLp53 activity gets impaired due to the dominant-negative effect exerted by the isoforms. The Δ133p53 or Δ160p53 isoforms either attenuate FLp53's transcription activity by hetero-tetramerization in a ratio higher than 1:1, or abolish it completely by aggregation. Since Δ133p53 and Δ160p53 exhibit much higher propensity for aggregation than FLp53, they sequester FLp53 in the cytoplasmic aggregates, leading to reduction in the amount of functional FLp53 in the nucleus. Aggregation also limits the availability of these isoforms in the nucleus. Thus, co-aggregation is the primary reason for dominant negative effect of the Δ133p53 or Δ160p53 isoforms on FLp53. It is important to note that the numbers of tetramers and aggregates depicted do not represent the actual quantities present in the cytoplasm and nucleus. **(B)** The balance between the expression level of the FLp53 and its isoforms Δ133p53 and Δ160p53 regulates FLp53 activity. Increased levels of Δ133p53 and Δ160p53 relative to FLp53, lead to stronger dominant-negative effect due to co-aggregation and hetero-tetramerization, while increased level of FLp53 than the isoforms Δ133p53 and Δ160p53 in cancer cells, leads to regaining of FLp53 function.